Using birefringence colors to evaluate a tunable liquid-crystal *q*-plate

David Marco[1], María del Mar Sánchez-López[1,*], Pascuala García-Martínez[2], and Ignacio Moreno[3]

[1]*Instituto de Bioingeniería, Universidad Miguel Hernández, 03202 Elche, Spain.*
[2]*Departamento de Óptica, Universidad de Valencia, 46100 Burjassot, Spain.*
[3]*Departamento de Ciencia de Materiales, Óptica y Tecnología Electrónica, Universidad Miguel Hernández, 03202 Elche, Spain.*
**mar.sanchez@umh.es*

Received XX Month XXXX; revised XX Month, XXXX; accepted XX Month XXXX; posted XX Month XXXX (Doc. ID XXXXX); published XX Month XXXX

Q-plates are geometrical phase elements that enable the realization of vector beams in simple and compact optical setups. In this work, we consider a tunable liquid-crystal commercial *q*-plate operative in the visible and near IR range and study its spectral and color birefringence properties under broadband illumination. We first characterize the spectral retardance function of the device in a wide range from 400-1600 nm and determine how it changes upon applied voltage. Then we evaluate the color transmission characteristics when inserting the *q*-plate between crossed and parallel linear polarizers. These color properties agree with the trajectory in the CIExy chromaticity diagram as the applied voltage changes. Finally, we demonstrate that a simple visual inspection of the transmitted birefringence color perceived when placing the *q*-plate between crossed polarizers can be used to obtain a rapid estimation of the *q*-plate retardance at given wavelength ranges. © 2018 Optical Society of America

http://dx.doi.org/10.1364/AO.99.099999

1. Introduction

Spatially-variant birefringent elements are becoming very popular to conceive new optical components, such as lenses, gratings, spiral phase plates, etc, in what has been named flat optical metasurfaces [1], geometric-phase elements [2,3], or fourth generation (4G) diffractive optical elements [4]. They are in essence diffractive waveplates where the orientation of the optical axis is spatially modulated in the plane of the waveplate. An early example was the liquid-crystal polarization converter, yielding light with axially distributed linear polarization [5]. Among these spatially-variant anisotropic elements, *q*-plates are specially interesting, since they can generate vortex beams and manipulate the orbital angular momentum (OAM) of light [6]. Furthermore, they can generate higher-order vector beams, where the polarization spatial pattern depends on the topological charge of the device (q) and on the input polarization [7]. Consequently, *q*-plates show relevant applications in many areas, like optical communications, where OAM and vector beams can be employed as additional degrees of freedom [8], materials processing [9] and particle manipulation [10].

When fabricated with liquid-crystals (LC), *q*-plates can be made tunable via a small voltage applied through coated electrodes [11,12]. While some research prototypes have been reported, to our knowledge, the only existing commercial tunable *q*-plate device is offered by the company ARCoptix [13]. Here we use this device in combination with a broadband light source to analyze the spectral content of the transmitted light as a function of voltage and the color patterns that are visible when it is placed in between polarizers.

While most of the work developed with *q*-plates involves monochromatic light, there is an increasing interest in the last years in their application with polychromatic light. For instance, axially symmetric Fresnel rhomb wave-plates have been used to generate achromatic vector beams [14,15] or achromatic angular momentum [16]. These devices use the achromatic retardance induced by Fresnel reflections. Alternatively, circular Bragg reflection from chiral uniaxial media can be exploited to generate reflective broadband *q*-plates [17]. Other approaches to achieve broadband vector beams require the use of complex optical systems based on spatial light modulators [18].

On the contrary, *q*-plates based on the material's retardance, as those made of liquid-crystals, exhibit an important retardance dispersion that affects the polarization efficiency conversion [19]. Tunable liquid-crystal *q*-plates have been demonstrated to operate at different wavelengths, including not only visible [11,12] but also near infrared (NIR) wavelengths [20]. It is also of interest when multiple wavelengths illuminate the *q*-plate simultaneously, as it is the case when generating a supercontinuum vector beam [21], or for their application in stimulated emission depletion (STED) microscopy, where maximum and zero polarization efficiency conversions are required simultaneously for two selected wavelengths [22]. In some cases, the *q*-plate can be operated at $\pi/2$ or at $3\pi/2$ retardance, thus generating hybrid vector beams [19,23]. This off-tuned operation is equivalent to superimposing a Gaussian beam with a pure vector beam and leads to

polarization-singular beams, also called Poincaré beams [24], that carry a C-point singularity at their center, as shown in [25].

Therefore, it is of great importance to accurately measure the device spectral retardance function $\phi(\lambda)$ in order to evaluate the polarization efficiency conversion for different wavelengths. The measurement of $\phi(\lambda)$ in regular linear retarders is typically done by placing the retarder between crossed and parallel linear polarizers, oriented at 45º with respect to the neutral axes, and illuminating the system with a light source of continuous broadband spectrum [26]. The transmitted light spectrum presents a typical oscillatory behavior with wavelength and can be measured by means of a spectrometer. Then, the spectral retardance function $\phi(\lambda)$ is calculated to give the best fit to the experimental data [27]. We have recently developed a system that combines two spectrometers, one for the visible (VIS) and another for the near infrared (NIR) ranges, that allows us to measure $\phi(\lambda)$ in a wide spectral range from 400 to more than 1600 nm [28]. However, this technique cannot be directly applied to q-plates, since their optical axis rotates azimuthally in the waveplate plane. Instead, it is more convenient to calibrate the q-plate retardance by inserting the device between circular polarizers [12,19].

The spectral variation of the light transmitted by anisotropic samples placed between crossed polarizers has been used for decades in mineralogy and microscopy. Illuminated under white light, low order anisotropic samples exhibit chromatic effects, known as birefringence colors or interference colors, that can be used to identify materials or minerals according to birefringence. This effect has been applied in liquid-crystal devices for instance to evaluate surface anchoring conditions [29], or to evaluate the modulation properties of twisted-nematic displays [30].

As it will be shown, liquid-crystal q-plate devices also exhibit such birefringence colors. In this work we analyze the birefringence color properties of a tunable liquid-crystal commercial q-plate, and how they can be used to estimate the voltage ranges where the device is tuned for maximum polarization conversion efficiency.

The paper is organized as follows: after this introduction, Section 2 briefly summarizes the q-plate theory. Then, in Section 3 we describe the optical system employed to measure the q-plate spectral retardance. We provide experimental results of the spectrum transmitted by the q-plate inserted between circular polarizers, and this information is used to retrieve the spectral retardance of the device. In Section 4, these spectra are related with the perceived color of the intensity pattern behind the analyzer: We discuss that, when placing the device in between crossed linear polarizers, the intensity pattern is equivalent to that provided by a tuned q-plate illuminated with monochromatic light, but the bright areas show a birefringence color that changes under the applied voltage. This color can be employed to estimate the retardance function of the device. Finally, Section 6 presents the conclusions of our work.

2. Q-plate theory

Q-plates are spatially-variable retarders whose optical axis rotate a fraction q of the azimuthal angle θ, i.e. $\theta = \arctan(y/x)$, thus acting as polarization converters [6]. This q value is always an integer or a semi-integer, so that the principal axis does not exhibit discontinuity lines on the plate, but only a defect in the center that sets the order ($\ell = 2q$) of the output vector beam. Therefore, these retarders can be described by the following Jones matrix [12]:

$$\mathbf{M_q}(\phi) = \mathbf{R}(-q\theta) \cdot \mathbf{W}(\phi) \cdot \mathbf{R}(+q\theta), \tag{1}$$

where the rotation matrix and the Jones matrix of a linear retarder with ϕ retardance and aligned along the $x - y$ coordinates are given, respectively, by:

$$\mathbf{R}(\theta) = \begin{pmatrix} \cos(\theta) & \sin(\theta) \\ -\sin(\theta) & \cos(\theta) \end{pmatrix}, \tag{2a}$$

and

$$\mathbf{W}(\phi) = \begin{pmatrix} \exp(+i\phi/2) & 0 \\ 0 & \exp(-i\phi/2) \end{pmatrix}. \tag{2b}$$

The q-plate Jones matrix obtained in Eq. (1) can then be written as:

$$\mathbf{M_q}(\phi) = \cos\left(\frac{\phi}{2}\right)\mathbf{I} + i\sin\left(\frac{\phi}{2}\right)\mathbf{Q_q} \tag{3}$$

where $\mathbf{I}$ represents the indentity matrix, and

$$\mathbf{Q_q} = \begin{pmatrix} \cos(2q\theta) & \sin(2q\theta) \\ \sin(2q\theta) & -\cos(2q\theta) \end{pmatrix} \tag{4}$$

is the Jones matrix of a tuned q-plate ($\phi = \pi$) [6]. Equation (3) shows that the q-plate maximum conversion efficiency is achieved whenever the retardance is an odd multiple of πradians, i.e., the retarder layer is a half-wave retarder. In this situation, the device transforms an input linear polarization onto an ℓ-order linearly polarized vector beam, and converts input circular polarization onto the opposite circular polarization adding an optical vortex of topological charge $\ell = \pm 2q$, where the sign depends on the helicity of the input circular polarization [6].

Equation (3) reveals that the action of a q-plate device with arbitrary retardance on an input polarization state is the superposition of the input state with the state resulting from the action of a regular tuned q-plate. The weight of each term, $\cos(\phi/2)$ and $\sin(\phi/2)$ respectively, depends on the actual retardance of the device. Interesting combinations for the generation of pure and hybrid vector beams were recently discussed [19].

Typically, liquid-crystal q-plates include a single low-order retarder layer, thus their spectral retardance decreases monotonically with wavelength according to the usual expression:

$$\phi = \frac{2\pi}{\lambda}\Delta n \cdot d, \tag{5}$$

where d is the LC layer thickness and $\Delta n = n_e - n_o$ is the birefringence of the LC material. If in addition the q-plate is electrically tunable, then the effective extraordinary index $n_e(V)$ is voltage dependent, and so it is the retardance $\phi(V)$. As reported in previous works, maximum retardance is achieved without applied voltage, while the retardance decreases for higher voltages [11,12].

Given the above considerations, the precise accurate determination of the spectral function retardance as a function of both the wavelength and the applied voltage $\phi(\lambda, V)$ is of great interest to determine the voltages where the q-plate provides the maximum polarization conversion efficiency for a given operating wavelength. Also, one may be interested in generating hybrid vector beams by operating the device at quarter-wave retardance.

3. Spectral characterization of the *q*-plate

The retardance characterization of a regular waveplate usually involves placing the retarder in between two crossed linear polarizers oriented at 45º with respect to the neutral axes [26-28]. However, in a q-plate the axes rotate azimuthally, and therefore this method cannot be applied directly. Instead, the q-plate retardance can be measured by placing the device in between crossed circular polarizers [12,19].

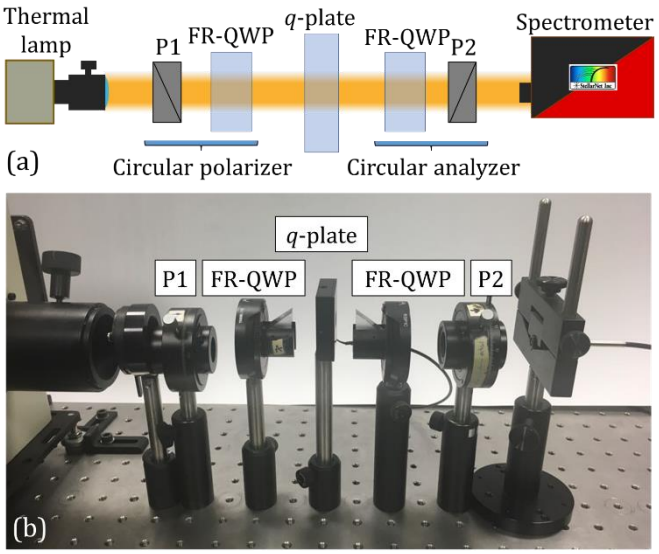

Fig. 1. (a). Scheme of the optical setup for the spectral characterization of the q-plate. (b) Picture of the experimental setup. P1 and P2 are linear polarizers, and FR-QWP are Fresnel rhombs quarter-wave retarders.

Following the procedure in [19] we have spectrally characterized a commercial LC q-plate from ARCoptix [13] (also called variable spiral plate) of q=0.5 and nominal operational wavelength range 400-1700 nm. The device retardation is controlled by an AC bias between 0V and 8V. The q-plate is inserted in between two broadband crossed or parallel circular polarizers and it is illuminated with light of a continuous spectrum, as shown in Fig. 1. As derived from Eq. (3), when the q-plate is illuminated with circular polarized light, the output state is a linear combination of right-circularly polarized (RCP) and left-circularly polarized (LCP) light. If we place a circular analyzer, which is crossed/parallel with respect to the input circular polarizer, the normalized transmission at the end of the system is given by:

$$i_{cros}^{cir} = \sin^2\left(\frac{\phi(\lambda)}{2}\right), \tag{6a}$$

$$i_{par}^{cir} = \cos^2\left(\frac{\phi(\lambda)}{2}\right). \tag{6b}$$

We illuminate the system with a quartz tungsten halogen (QTH) lamp from Oriel (model 66882), with adjustable power from 10 to 250 watts. It provides light of continuous broadband spectrum from 400 nm to more than 1600 nm. We build the broadband circular polarizers by orienting two calcite Glan-Taylor cube polarizers (Edmund Optics, with an operation range from 350 to 2200 nm) at 45° with respect to the neutral axes of two achromatic quarter-wave Fresnel rhombs. The Fresnel rhombs (Thorlabs, model FR600QM) exhibit a maximum retardance deviation of less than 3° [31] in the 400 to 1550 nm range. The spectral transmission of the whole system is measured by two different spectrometers. For the visible range, we capture the beam with a STN-F600_UVVIS-SR optical fiber that sends the light to a VIS spectrometer (Stellar-Net, model STN-BLK-C-SR), which measures light from 200 nm to 1080 nm. To measure in the near infrared, we send the beam directly to a NIR spectrometer (Stellar-Net, model STE-RED-WAVE-NIR-512-25), which operates in the 900 nm to 1700 nm range. We measured the NIR data with the lamp set at a power of 20 watts, while the VIS data required a power of 40 watts in order to have more light in the violet region.

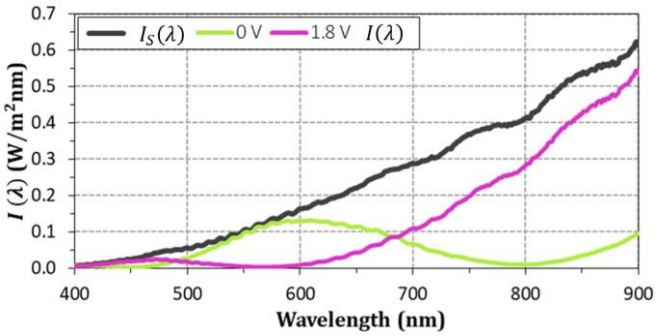

Fig. 2. Spectrum $I_S(\lambda)$ of the maximum transmission of the optical system with the QTH lamp power set at 40 W (black line). This spectrum was obtained by adding the two irradiances measured for the q-plate between crossed and parallel circular polarizers with no bias voltage. Transmitted spectrum $I(\lambda)$ of the q-plate between crossed circular polarizers at 0V (green line) and 1.8V (pink line).

Figure 2 shows the spectrum $I_S(\lambda)$ of the maximum possible transmission of the optical system (q-plate between circular polarizers), measured in the visible range with the QTH lamp power set at 40 W. It was obtained by adding for each wavelength the output irradiance values for crossed and parallel circular polarizers. It follows the typical spectrum of a QTH lamp, where the irradiance diminishes gradually as the wavelength decreases. The spectrum $I(\lambda)$ of the light transmitted by the q-plate system between polarizers is then given by:

$$I(\lambda) = i(\lambda) I_S(\lambda), \tag{7}$$

where $i(\lambda)$ is the normalized spectral transmission, which depends on the selected polarization configuration. For crossed/parallel circular polarizers, $i(\lambda)$ is given by Eqs. (6). We consider $I(\lambda)$ in the next section for the color evaluation of the q-plate device.

However, as mentioned before, we extend the spectral characterization range by adding in NIR measurements. Figure 3 shows the normalized spectral transmission when the q-plate is illuminated between crossed circular polarizers, for different applied voltages. Blue points correspond to data measured with the VIS spectrometer, while red points correspond to data captured with the NIR spectrometer. These data were obtained by measuring the spectrum for crossed circular polarizers and for parallel circular polarizers. Then the spectrum for crossed polarizers was divided by the addition of the spectra for crossed and parallel polarizers. These calculations were made for every wavelength measured by the spectrometers, and the resulting normalized curve is directly comparable to Eq. (6a).

The curves in Fig. 3 show the expected behavior. The transmitted spectrum shows oscillations originated by the wavelength dependence of the retardance (Eq. (5)) and the sinusoidal transmission (Eq. (6a)). The maxima in the curves in Fig. 3 denote the wavelengths where the retardance is an odd multiple of π. At these wavelengths there is a full conversion from a homogeneous polarized beam to the corresponding vector beam. On the contrary, the minima of the curves denote the wavelengths for which the retardance is an even number of π. For these wavelengths, the q-plate shows a null polarization conversion, according to Eq. (3). Note that the experimental data do not reach the values 0 or 1 in the violet region. We attribute this effect to the high noise contribution, due to the weak intensity of the light provided by the lamp in this region. Nevertheless, the data in Fig. 3 can be used to fit the spectral retardance function.

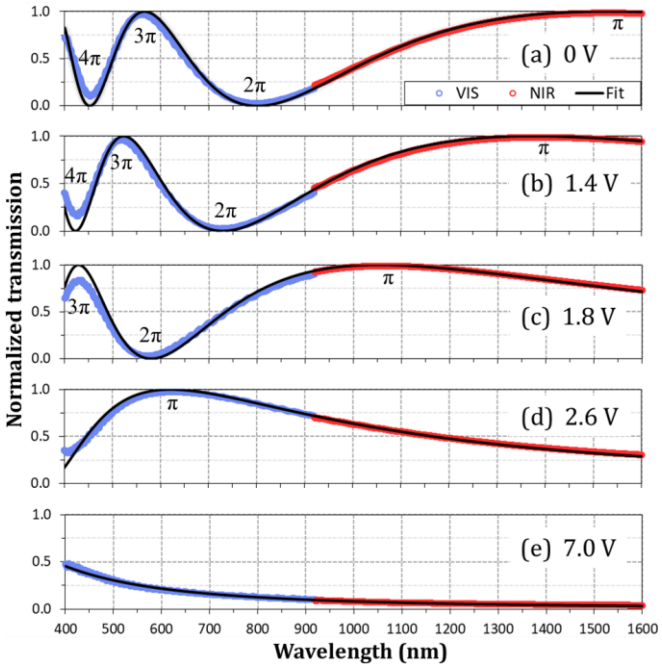

Fig. 3. (a)–(e) Normalized spectral transmission of the q-plate between crossed circular polarizers for bias voltages: 0 V, 1.4 V, 1.8 V, 2.6 V and 7.0 V. Measured data are shown in blue and red for the VIS and NIR spectrometers, respectively. Black curves denote the calculated transmission that best fit the experimental data.

The retardance for each wavelength and for each measured voltage is retrieved from:

$$\phi(\lambda) = 2\arcsin\left(\sqrt{i_{cros}^{cir}(\lambda)}\right), \qquad (8)$$

which is derived from Eq. (6a). Since this equation only provides phase values between 0 and π radians, we impose the condition that the retardance must be a continuous and monotonically decreasing function of wavelength [28], in agreement with Eq. (5). Together with the knowledge that the retardance decreases as the voltage increases, it is thus possible to easily identify the order of the retarder. Starting from the maximum applied voltage (Fig. 3(e)), where only minimal residual retardance is observed, the retardance increases for lower voltages. This allows identifying the retardance of π radians as the maximum located around 600 nm for V=2.6V (Fig. 3(d)). This maximum shifts to wavelengths around 1050 nm, 1400 nm and 1600 nm when the voltage decreases to 1.8V (Fig. 3(c)), 1.4V (Fig. 3(b)), and to zero (Fig. 3(a)). Following this procedure it is possible to easily identify other wavelengths where the retardance is $\phi(\lambda) = m\pi$, as indicated in Fig. 3.

Note that this analysis is relevant for the application of q-plates in STED microscopy [22]. In that case, the sample must be illuminated with a Gaussian beam of wavelength that excites the fluorescence, and a vortex beam of a second wavelength that inhibits fluorescence –except within the optical singularity–. Different pairs of wavelengths can be used. Different pairs of wavelengths appropriate to be applied with different dyes common in STED microscopy were reported by Yan *et al* [22]. Among all the possible pairs indicated in that reference, we find that the ARCoptix q-plate would only be useful for STED microscopy with the 532-440 nm pair and setting the bias voltage at about 1.3V. Namely, we find maximum polarization conversion efficiency at 537 nm (fluorescence inhibition wavelength) and minimum efficiency at 438 nm (fluorescence activating wavelength). Note that a q-plate made of the same liquid-crystal, but with a thicker layer, would provide more oscillations in the spectrum, and therefore could be used for STED microscopy at a wider number of wavelength pairs [22,32].

Figure 4(a) shows the spectral retardance fitted from the spectra in Fig. 3. We assume that the refractive indices of the retarder can be described by a Cauchy dispersion relation [33]. Therefore, we fit the experimental spectral retardance function given in Eq. (8) to $\phi_{fit}(\lambda) = A/\lambda + B/\lambda^3$, and find the constants A and B that best recover the experimental retardance. The values of the fitted retardance are then used into Eq. (6) in order to calculate the normalized transmission, which is plotted as a black continuous line in Fig. 3 together with the experimental data.

The curves in Fig. 4(a) show the expected behavior, where the retardance progressively decreases with wavelength and with the applied voltage. We select four wavelengths and show their retardance dependence with voltage in Fig. 4(b). These wavelengths correspond to the violet diode laser (405 nm), the He-Ne laser (633 nm), a near IR laser (980 nm) and the optical communications band (1550 nm). Of course, any other wavelength in the measured range could be evaluated. Slight discontinuities in the retardance curve for 405 nm are observed, that we attribute to the low signal-to-noise ratio at this wavelength, due to the low intensity provided by the thermal lamp at short wavelengths.

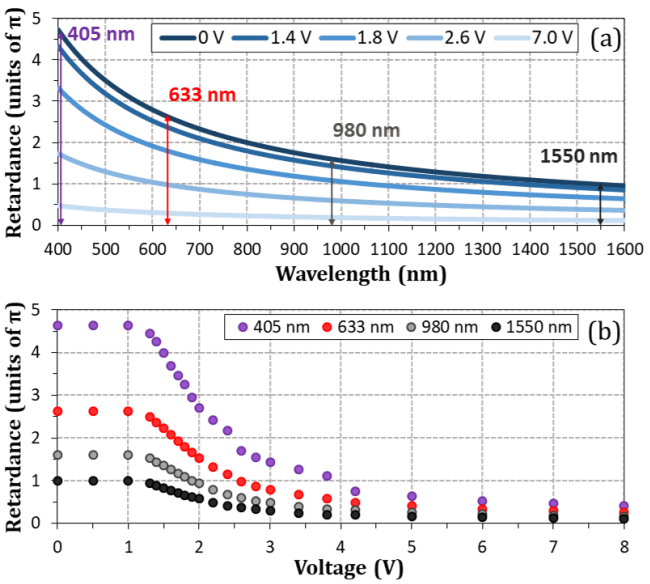

Fig. 4. (a) Spectral retardance of the q-plate for various voltages: (b) Q-plate retardance versus voltage for four selected wavelengths.

The previous results demonstrate a systematic and accurate experimental procedure to derive the spectral retardance function of the q-plate. The variations with voltage of the spectral transmission have implications in the color that is perceived when the device is placed between linear polarizers. In the next section we analyze these effects.

4. Study of the birefringence colors

Birefringence colors have been known for decades to give information about the spectral retardance of materials. In this section we relate the color properties of the light transmitted by the q-plate placed in between polarizers with the spectral transmission results discussed in the previous section. Note that the only relevant information for this purpose is the illuminant spectrum (Fig. 2) and the transmission in the visible spectral region, so we can at this point ignore the NIR measurements.

Birefringence colors are observed when placing the sample between crossed linear polarizers. Note that in this situation the identity matrix

term in Eq. (3) does not play any role. Since this term does not transform the input polarization, its corresponding output will be blocked by the output analyzer. It is a simple Jones matrix calculation to derive that the intensity pattern transmitted by the system composed by the q-plate inserted in between crossed linear polarizers is now given by

$$i_{cros}^{lin} = \sin^2\left(\frac{\phi(\lambda)}{2}\right)\sin^2(2q\theta). \quad (9)$$

The term $\sin^2(2q\theta)$ in this equation yields an azimuthal distribution of the transmitted intensity, with the typical two-lobe dark pattern generated by linearly polarized first-order vector beams illuminating a linear analyzer. The above relation indicates that the q-plate inserted between crossed linear polarizers shows the same intensity pattern with two dark lobes for all wavelengths, and only the intensity of the bright lobes changes with wavelength according to the factor $\sin^2(\phi(\lambda)/2)$. Note that this factor is exactly the one in Eq. (6a) which is shown in Fig. 3. But when the q-plate is located between crossed circular polarizers, the transmission is spatially uniform as provided by Eq. (6a), which is devoid of the azimuthal term.

A q-plate inserted between linear polarizers generates a characteristic spatial pattern in the form of azimuthal lobes when illuminated with monochromatic light. Eq. (9) reveals that exactly the same pattern will be generated for all wavelengths if the q-plate is between crossed linear polarizers. Therefore, in this situation, if the system is illuminated with polychromatic light, it will present a uniform color in the bright lobes, fixed by the spectral transmission curves shown in Fig. 3. Note that this is the case only when the linear polarizers are crossed. In other configurations, where the polarizers would not be crossed, the identity term in Eq. (3) will contribute also to the transmitted light, providing thus a color variation along the azimuthal pattern.

As shown in the previous section, the ARCoptix q-plate retardance can be tuned via an applied voltage, and so does the normalized transmission. Therefore, the color of these bright areas can be varied with voltage, and it can be used to achieve a fast evaluation of the operation conditions of the device.

This is shown in Fig. 5. Figure 5(a) shows pictures of the q-plate placed between two crossed linear polarizers, that were taken with a Nikon D3300 photographic camera. All images display the same intensity pattern with two bright lobes and two dark lobes, as expected for a q-plate with q=0.5. Note how the color of the bright areas changes as different voltages are applied to the device. However, the color is always uniform. The two dark lobes indicate the spatial regions where the output polarization is crossed with respect to the transmission axis of the analyzer.

This is not the case of Fig. 5(b), where the q-plate is now placed between parallel linear polarizers. The intensity pattern obtained for the parallel linear polarizers configuration is:

$$i_{par}^{lin} = \cos^2\left(\frac{\phi(\lambda)}{2}\right) + \sin^2\left(\frac{\phi(\lambda)}{2}\right)\cos^2(2q\theta). \quad (10)$$

Note that this expression contains two terms: the first term is spatially uniform, and thus provides a uniform background; the second term, varies with the azimuthal angle with a spatial distribution that is complementary to the one in Eq. (9). As a consequence, now white lobes appear where dark areas were present with crossed polarizers. Therefore, the azimuthal color variation now changes from white to a color complementary to that observed with crossed polarizers. This is similar to the birefringent colors observed with linear retarders [34], but the q-plate generates them along the azimuthal coordinate.

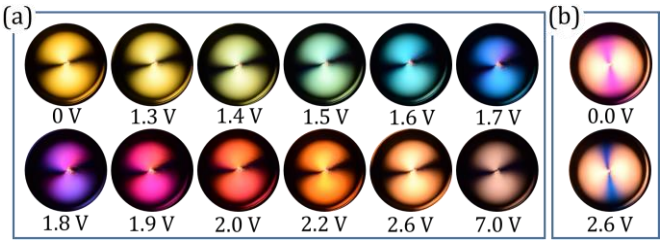

Fig. 5. Photographs of the q-plate with various applied voltages and placed between (a) crossed and (b) parallel linear polarizers.

In order to evaluate the color properties shown in Fig. 5(a), first we calculate the tristimulus values of the light transmitted at the end of the system with crossed polarizers by projecting the measured spectral irradiance $I(\lambda, V)$ onto the basis of the color matching functions. According to the CIE 1931-XYZ standard observer, the tristimulus values can be obtained as [35]:

$$X(V) = \int_0^\infty I(\lambda, V)\bar{x}(\lambda)\mathrm{d}\lambda, \quad (11a)$$

$$Y(V) = \int_0^\infty I(\lambda, V)\bar{y}(\lambda)\mathrm{d}\lambda, \quad (11b)$$

$$Z(V) = \int_0^\infty I(\lambda, V)\bar{z}(\lambda)\mathrm{d}\lambda, \quad (11c)$$

where $\bar{x}(\lambda)$, $\bar{y}(\lambda)$ and $\bar{z}(\lambda)$ are the color matching functions, that represent the response of the human eye to an arbitrary electromagnetic spectrum. The curve $I(\lambda, V)$ is given by Eq. (7), considering, for every voltage value, the corresponding normalized transmission obtained for crossed circular polarizers (Eq. (6a)). The chromaticity coordinates are calculated as

$$x(V) = \frac{X(V)}{X(V)+Y(V)+Z(V)}, \quad (12a)$$

$$y(V) = \frac{Y(V)}{X(V)+Y(V)+Z(V)}, \quad (12b)$$

$$z(V) = \frac{Z(V)}{X(V)+Y(V)+Z(V)}. \quad (12c)$$

Then, the perceived color as the applied voltage changes is described by the coordinates $x(V)$ and $y(V)$ of the corresponding point in the CIExy chromaticity diagram. Figure 6(a) shows this diagram and the trajectory of the corresponding chromaticity coordinates as the applied voltage increases.

It is interesting to remark that these birefringence colors are visible when the q-plate retarder exhibits a first-order retardance. The spectral normalized transmission in Fig. 3 shows that a 2π retardance (identified as the minimum transmission) transits the visible wavelengths for voltages between 1.5V and 2.0V. For smaller retardances, the spectrum varies so slowly that the transmitted light would appear white. For higher-order retardances, the transmitted spectrum oscillates so rapidly that there is enough energy in all regions of the visible light, and again it would look white. However, for the first-order retardance, the birefringence colors are clearly visible. This is therefore an extremely simple method to determine when the retardance is approximately 2π.

Finally, in order to fully characterize the color perception of the output transmittance, the information about the brightness is also required and that is determined by the illuminance function $I_V(V)$, calculated as:

$$I_V(V) = K_n Y(V), \quad (13)$$

where K_n =683 lm/W denotes the maximum photopic luminous efficiency of the human eye. Figure 6(b) shows the illuminance function versus the applied voltage. The higher value for illuminance corresponds to 1.4V. At this value, as can be appreciated in Fig. 3(b), most of the transmitted light is in the green region of the visible spectrum, where the maximum visual response of the human eye lays. The illuminance lowest value is obtained for a voltage of 1.8V where, as Fig. 3(c) shows, the spectral transmittance reaches its lowest value around 560 nm. In this case, the higher contribution of the transmitted light is in the blue and red regions of the visible spectrum, which contribute less to the illuminance. Note that this transition around the minimum illuminance corresponds to a detour of the $y(x)$ trajectory in Fig. 6(a) around the cyan-blue-magenta region. Thus, the minimum illuminance is again a sign that the 2π retardance transits the center of the visible spectrum.

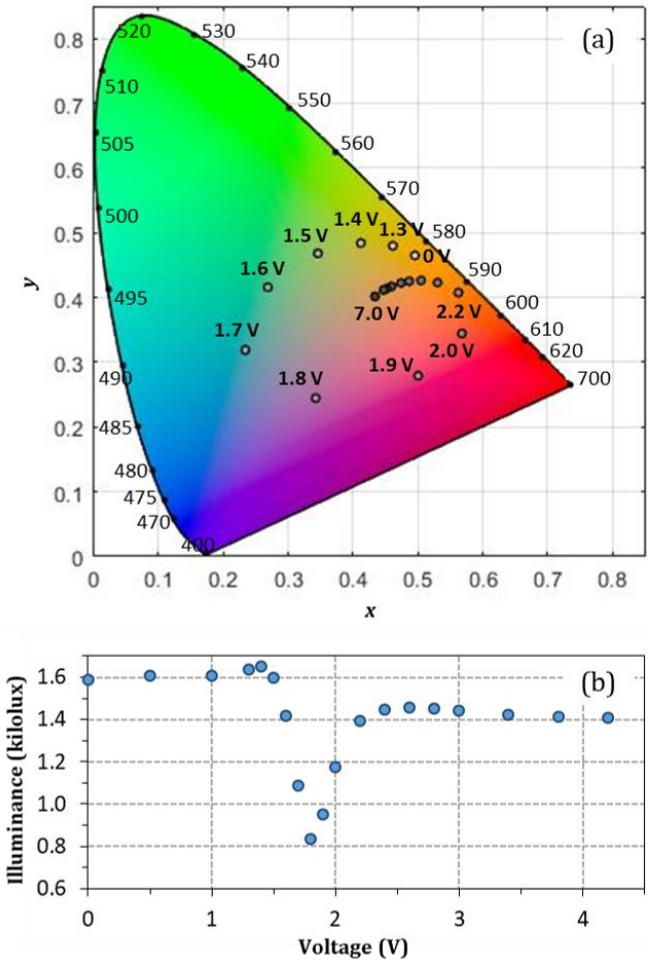

Fig. 6 (a) Chromaticity CIExy diagram for different voltages. The voltage values not indicated for some points are: 2.4V, 2.6V, 2.8V, 3.0V, 3.4V, 3.8V and 4.2V. (b) Illuminance for different applied voltages.

5. Conclusions

In summary, a study of the spectral and color properties of a tunable liquid-crystal commercial q-plate operating in the VIS and NIR range has been presented. First, we apply a previously reported experimental system to characterize the q-plate retardance as a function of wavelength and voltage in the range from 400 to 1600 nm. For that purpose, the q-plate was placed between crossed and parallel circular polarizers built with quarter-wave Fresnel rhombs and Glan-Taylor linear polarizers. The spectral transmission curves obtained in such a wide spectral range allows easily identifying the order of the retardance by simply regarding the evolution of the transmission minima and maxima as the voltage changes. A pair of wavelengths and the required bias voltage is identified for a possible application of this commercial q-plate in STED microscopy.

In the second part of the paper, we provided a comprehensive description of the color properties perceived upon changing the bias voltage when placing the q-plate between linear polarizers. This is a common situation for a q-plate under monochromatic light. Here instead, the device is illuminated with broadband light. We demonstrated that the typical intensity pattern consisting of azimuthal dark lobes (displayed by a q-plate tuned at π retardance) is obtained for all wavelengths, provided the input and output linear polarizers are crossed. In this situation, the bright lobes exhibit a uniform color, with the birefringence color being determined by the spectral transmission. These color properties are accounted for by the trajectory in the CIExy chromaticity diagram as the applied voltage changes.

Finally, we have shown a strong variation of the birefringence color when the first-order retardance transits the visible region of the spectrum. Thus, this can be considered as an extremely simple method to determine when the q-plate is reaching a retardance of about 2π radians, a technique capable to be used even with the naked eye. Alternatively, low cost spectrometers [36] could also be applied to make the kind of measurements here presented.

Funding Information. This research has been funded by Generalitat Valenciana, Conselleria d'Educació, Investigació, Cultura i Esport (PROMETEO-2017-154) and Ministerio de Economía, Industria y Competitividad of Spain and European Union (MIMECO/FEDER funds, grant FIS2015-66328-C3-3-R).

References

1. N. Yu and F. Capasso, "Flat optics with designer metasurfaces", Nat. Materials **13**, 139–150 (2014).
2. J. Kim, Y. Li, M.N. Miskiewicz, C. Oh, M.W. Kudenov, and M.J. Escuti, "Fabrication of ideal geometric-phase holograms with arbitrary wavefronts", Optica **2**(11), 958-964 (2015).
3. R. Drevinskas and P.G. Kazansky, "High-performance geometric phase elements in silica glass"; APL Photonics **2**, 066104 (2017).
4. L. De Sio, D. E. Roberts, Z. Liao, S. Nersisyan, O. Uskova, L. Wickboldt, N. Tabiryan, D.M. Steeves, and B. R. Kimball, "Digital polarization holography advancing geometrical phase optics", Opt. Express **24**(16), 18297-18306 (2016).
5. M. Stalder and M. Schadt, "Linearly polarized light with axial symmetry generated by liquid-crystal polarization converters," Opt. Lett. **21**, 1948-1950 (1996).
6. L. Marrucci, C. Manzo, and D. Paparo, "Optical spin-to-orbital angular momentum conversion in inhomogeneous anisotropic media," Phys. Rev. Lett. **96**, 163905 (2006).
7. F. Cardano, E. Karimi, S. Slussarenko, L. Marrucci, C. de Lisio, and E. Santamato, "Polarization pattern of vector vortex beams generated by q-plates with different topological charges", Appl. Optics **51**(10), C1-C6 (2012).
8. G. Milione, M. P. J. Lavery, H. Huang, Y. Ren, G. Xie, T. A. Nguyen, E. Karimi, L. Marrucci, D. A. Nolan, R. R. Alfano, and A. E. Willner, "4×20 Gbit/s mode division multiplexing over free space using vector modes and a q-plate mode (de)multiplexer," Opt. Lett. **40**, 1980-1983 (2015).
9. S. R. Nersisyan, N. V. Tabiryan, D. Mawet, and E. Serabyn, "Improving vector vortex waveplates for high-contrast coronagraphy", Opt. Express **21**, 8205-8213 (2013).
10. B. J. Roxworthy, K. C. Toussaint Jr., "Optical trapping with π-phase cylindrical vector beams", New J. Phys. **12**, 073012 (2010).

11. S. Slussarenko, A. Murauski, T. Du, V. Chigrinov, L. Marrucci, and E. Santamato, "Tunable liquid crystal *q*-plates with arbitrary topological charge," Opt. Express **19**, 4085-4090 (2011).
12. J. A. Davis, N. Hashimoto, M. Kurihara, E. Hurtado, M. Pierce, M. M. Sánchez-López, K. Badham, and I. Moreno, "Analysis of a segmented *q*-plate tunable retarder for the generation of first-order vector beams," Appl. Opt. **54**, 9583-9590 (2015).
13. http://www.arcoptix.com/Q_Plate.htm
14. T. Wakayama, K. Komaki, Y. Otani, and T. Yoshizawa, "Achromatic axially symmetric wave plate", Opt. Express **20**(28), 29260-29265 (2012).
15. T. Wakayama, O. G. Rodríguez-Herrera, J. Scott Tyo, Y. Otani, M. Yonemura, and T. Yoshizawa, "Generation of achromatic, uniform-phase, radially polarized beams", Opt. Express **22**(3), 3306-3315 (2014).
16. F. Bouchard, H. Mand, M. Mirhosseini, E. Karimi, and R. W. Boyd, "Achromatic orbital angular momentum generator", New J. Phys. **16**, 123006 (2014).
17. M. Rafayelyan and E. Brasselet, "Bragg-Berry mirrors: reflective broadband *q*-plates", Opt. Lett. 41(17), 3972-3975 (2016).
18. K. J. Mitchell, N. Radwell, S. Franke-Arnold, M. J. Padgett, and D. B. Phillips, "Polarisation structuring of broadband light", Opt. Express **25**(21), 25079-25089 (2017).
19. M. M. Sánchez-López, I. Abella, D. Puerto-García, J. A. Davis, I. Moreno, "Spectral performance of a zero-order liquid-crystal polymer commercial *q*-plate for the generation of vector beams at different wavelengths," Opt. Laser Technol. **106**, 168–176 (2018).
20. K. Badham, S. Delaney, N. Hashimoto, M. M. Sánchez-López, M. Kurihara, A. Tanabe, I. Moreno, and J. A. Davis, "Generation of vector beams at 1550 nm telecommunications wavelength using a segmented *q*-plate," Opt. Eng. **55**, 030502 (2016).
21. Y. S. Rumala, G. Milione, T. A. Nguyen, S. Pratavieira, Z. Hossain, D. Nolan, S. Slussarenko, E. Karimi, L. Marrucci, and R. R. Alfano, "Tunable super-continuum light vector vortex beam generator using a *q*-plate," Opt. Lett. **38**, 5083-5086 (2013).
22. L. Yan, P. Gregg, E. Karimi, A. Rubano, L. Marrucci, R. Boyd, and S. Ramachandran, "Q-plate enabled spectrally diversed orbital-angular-momentum conversion for stimulated emission depletion microscopy," Optica **2**, 900-903 (2015).
23. M. Beresna, M. Gecevičius, P. G. Kazansky, and T. Gertus, "Radially polarized optical vortex converter created by femtosecond laser nanostructuring of glass", Appl. Phys. Lett. **98**, 211101 (2011).
24. A. M. Beckley, T. G. Brown and M. A. Alonso, "Full Poincaré beams", Opt. Express **18**(10), 10777-10785 (2010).
25. F. Cardano, E. Karimi, L. Marrucci, C. de Lisio, and E. Santamato, "Generation and dynamics of optical beams with polarization singularities", Opt. Express **21**(7), 8815-8820 (2013).
26. M. Emam-Ismail, "Spectral variation of the birefringence, group birefringence and retardance of a gypsum plate measured using the interference of polarized light," Opt. Laser Technol. **41**, 615-621 (2009).
27. A. Vargas, R. Donoso, M. Ramírez, J. Carrión, M. M. Sánchez-López and I. Moreno, "Liquid crystal retarder spectral retardance characterization based on a Cauchy dispersion relation and a voltage transfer function", Opt. Review, **20**(5), 378-384 (2013).
28. A. Messaadi, M. M. Sánchez-López, P. García-Martínez, A. Vargas, and I. Moreno, "Optical system for measuring the spectral retardance function in an extended range," J. Eur. Opt. Soc. – Rapid Pub. **12**, 21 (2016).
29. Y. Zou, J. Namkung, Y. Lin, D. Ke, and R. Lindquist, "Interference colors of nematic liquid crystal films at different applied voltages and surface anchoring conditions", Opt. Express **19**(4), 3297-3303 (2011).
30. J. L. Martínez, P. García-Martínez, M. M. Sánchez-López, I. Moreno, "Accurate color predictability based on a spectral retardance model of a twisted-nematic liquid-crystal display", Opt. Commun. **284**, 2441–2447 (2011).
31. https://www.thorlabs.com/newgrouppage9.cfm?objectgroup_id=154 (visited 2018/11/25).
32. https://nanobiophotonics.mpibpc.mpg.de/dyes/ (visited 2018/11/25).
33. J. Li, C.H. Wen, S. Gauza, R. Lu, and S.T. Wu, "Refractive indices of liquid crystals for display applications", J. Displ. Technol. **1**, 51–61 (2005).
34. P. Velásquez, M. M. Sánchez-López, I. Moreno, D. Puerto, and F. Mateos, "Interference birefringent filters fabricated with low cost commercial polymers", Am. J. Phys. **73**(4), 357-361 (2005).
35. D. Malacara, Color Vision and Colorimetry, SPIE Press, Bellingham (2002).
36. T. C. Muñoz Hernández, E. González-Valencia, P. Torres, D. L. Aristizábal Ramírez, "Low-cost spectrometer for educational applications using mobile devices"; Opt. Pura Apl. **50**(3), 221-228 (2017).